Near-infrared remotely triggered drug-release strategies for cancer treatment

Amanda M. Goodman[a], Oara Neumann[b], Kamilla Nørregaard[c], Luke Henderson[a], Mi-Ran Choi[d], Susan E. Clare[d], and Naomi J. Halas[a,b,e,f,1]

[a]Department of Chemistry, Rice University, Houston, TX 77005; [b]Department of Electrical and Computer Engineering, Rice University, Houston, TX 77005; [c]The Niels Bohr Institute, University of Copenhagen, 2100 Copenhagen, Denmark; [d]Department of Surgery, Feinberg School of Medicine, Northwestern University, Chicago, IL 60611; [e]Department of Physics and Astronomy, Rice University, Houston, TX 77005; and [f]Department of Bioengineering, Rice University, Houston, TX 77005

Contributed by Naomi J. Halas, October 6, 2017 (sent for review July 24, 2017; reviewed by Omid C. Farokhzad and Vincent Rotello)

Remotely controlled, localized drug delivery is highly desirable for potentially minimizing the systemic toxicity induced by the administration of typically hydrophobic chemotherapy drugs by conventional means. Nanoparticle-based drug delivery systems provide a highly promising approach for localized drug delivery, and are an emerging field of interest in cancer treatment. Here, we demonstrate near-IR light-triggered release of two drug molecules from both DNA-based and protein-based hosts that have been conjugated to near-infrared-absorbing Au nanoshells (SiO_2 core, Au shell), each forming a light-responsive drug delivery complex. We show that, depending upon the drug molecule, the type of host molecule, and the laser illumination method (continuous wave or pulsed laser), in vitro light-triggered release can be achieved with both types of nanoparticle-based complexes. Two breast cancer drugs, docetaxel and HER2-targeted lapatinib, were delivered to MDA-MB-231 and SKBR3 (overexpressing HER2) breast cancer cells and compared with release in noncancerous RAW 264.7 macrophage cells. Continuous wave laser-induced release of docetaxel from a nanoshell-based DNA host complex showed increased cell death, which also coincided with nonspecific cell death from photothermal heating. Using a femtosecond pulsed laser, lapatinib release from a nanoshell-based human serum albumin protein host complex resulted in increased cancerous cell death while noncancerous control cells were unaffected. Both methods provide spatially and temporally localized drug-release strategies that can facilitate high local concentrations of chemotherapy drugs deliverable at a specific treatment site over a specific time window, with the potential for greatly minimized side effects.

chemotherapy | cancer | drug release | near-infrared | nanoparticle

Breast cancer is the leading cause of cancer deaths among women worldwide, accounting for 1.7 million new diagnoses in 2012 (1). Current treatments for breast cancer include a combination of surgery, radiation, chemotherapy, molecularly targeted, and antihormonal therapeutics (2, 3). One promising approach in cancer treatment is the use of gold-based nanostructures, whose strong optical absorption is due to their plasmon resonance, to provide safe and effective light-based therapeutics. Plasmonic nanostructures are advantageous due to their unique optical properties, low toxicity, in vivo stability, and enhanced tumor uptake (4–10). One approach uses near-infrared (IR) light to heat silica core-gold shell nanoshells (NS) photothermally to locally ablate tumors, which has been shown to lead to tumor remission in mice at rates above 90% (11–13). In another approach, near-IR light is used to selectively release oligonucleotides and molecules from the nanoparticle surface for gene therapy and drug delivery (14–17). This latter approach also has highly promising potential for cancer therapy, where high local concentrations of drugs could be released remotely, on demand, in a spatially localized region such as the site of a tumor or metastatic disease, while the overall systemic dosage to a patient would remain relatively low. This approach could unleash the potential of known highly effective drugs that could otherwise induce toxicity at high systemic doses.

A wide range of host molecules have been developed to provide specific binding of therapeutic molecules for nanoparticle-based drug delivery (18–21). DNA and proteins are of particular interest, since they can be readily conjugated for attachment to gold nanoparticle surfaces, and their structures can be tailored for uptake of drug molecules in a host–guest manner (22–24). Host-conjugated nanoparticles can provide efficient internalization into cells and provoke less of an immune response than free drug molecules (25–29). For remotely triggered drug delivery, equally important is the nanoparticle's light-induced drug-release mechanism. Recently we have shown that continuous-wave (CW)-induced light-triggered release requires the bulk temperature of the illuminated nanoparticle to rise above the thiolated *ds*DNA dehybridization temperature to release *ss*DNA, while light-induced release using femtosecond near-IR laser pulses breaks the Au–S bond that binds the DNA to the nanoparticle with no measurable bulk temperature increase (30).

Here we investigate near-IR light-triggered release of therapeutic molecules using two potential host molecules, thiolated dsDNA and the protein human serum albumin (HSA), conjugated onto Au NS to form two optically addressable drug delivery complexes, NS@DNA and NS@HSA, respectively. These complexes play host to two FDA-approved breast cancer drugs: docetaxel (DTX) and lapatinib (LAP) molecules. DTX is an antimitotic chemotherapy drug that binds to the inside of microtubules preventing

Significance

Gold-based nanoparticles that absorb near-infrared light have shown the potential to selectively target and treat cancer through highly efficient light-to-heat conversion. This study shows that gold-based nanoparticles can be coated with drug-bearing host biomolecules for remotely triggerable release. Near-infrared light-triggered release of docetaxel from a nanoshell-based DNA host complex, and lapatinib from nanoshell-based DNA and human serum albumin host complexes, is demonstrated. There is a strong dependence upon the type of near-infrared illumination—continuous wave or pulsed—specific to the drug-laden host molecules. Localizing drug delivery both spatially and temporally by combining nanoshell-based complexes and pulsed-laser irradiation is a promising strategy for highly controlled drug delivery that can apply to a myriad of therapeutic applications.

Author contributions: A.M.G., O.N., S.E.C., and N.J.H. designed research; A.M.G., O.N., K.N., L.H., and M.-R.C. performed research; A.M.G., O.N., M.-R.C., and S.E.C. analyzed data; and A.M.G., O.N., L.H., M.-R.C., S.E.C., and N.J.H. wrote the paper.

Reviewers: O.C.F., Brigham and Women's Hospital; and V.R., Harvard Medical School.

The authors declare no conflict of interest.

[1]To whom correspondence should be addressed. Email: halas@rice.edu.

This article contains supporting information online at www.pnas.org/lookup/suppl/doi:10.1073/pnas.1713137114/-/DCSupplemental.

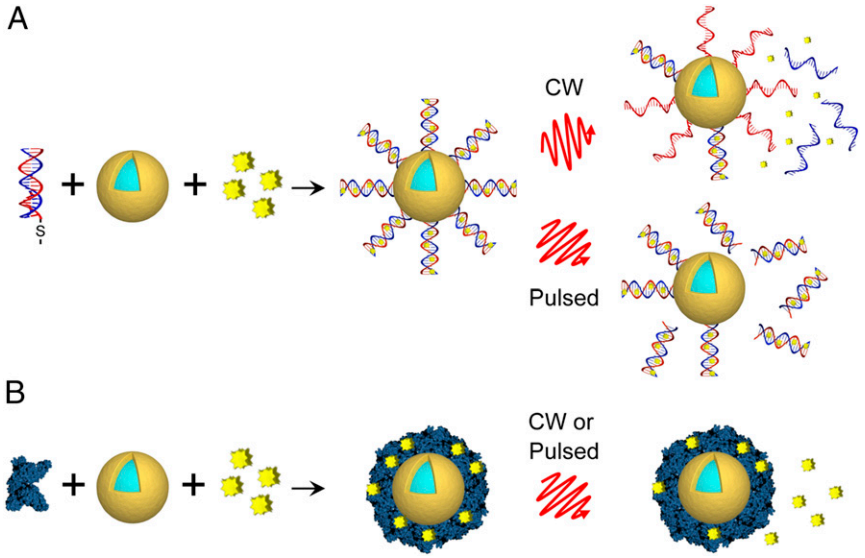

Scheme 1. Nanocomplex formation. (*A*) Formation of NS@DNA@drug nanocomplex by functionalization of NS with thiolated *ds*DNA through Au–thiol bonds, followed by attachment of drug molecules. Release triggered by CW irradiation results in *ds*DNA dehybridization and release of the drug, while pulsed irradiation results in Au–S bond breakage and release of the *ds*DNA–drug complex. (*B*) Formation of NS@HSA@drug by coating NS with HSA, and attachment of drug molecules. Drug release from the protein is triggered by CW or pulsed irradiation.

their disassembly, which disrupts cell division (31). LAP is a tyrosine kinase inhibitor that works by binding to the intracellular ATP binding site of the tyrosine kinase domain of HER2 blocking phosphorylation (32). Growth factor receptors, such as HER2, are proteins on the cell surface that signal it to grow and divide: LAP acts to block the HER2 protein, overexpressed on some forms of breast cancer, from signaling cell growth (33). Near-IR light-induced intracellular release was performed in MDA-MB-231 and SKBR3 (overexpresses HER2) breast cancer cells and compared with release in noncancerous RAW 264.7 macrophage cells. Macrophages were used as the control cells, as they have been shown to be able to phagocytose nanoparticles and deliver them to metastatic tumors where photothermal therapy can be applied (34, 35). Future studies would involve macrophages delivering these particles for targeted in vivo drug release. Cellular cytotoxicity was compared when drugs were released from the NS@DNA and the NS@HSA complexes. Two methods for near-IR light-triggered release, CW laser light at 1.5 W incident power and pulsed-laser irradiation, where 160-fs near-IR laser pulses at 25 mW average power were used. Our study shows that NS@DNA host complexes release their drug payload using CW laser light, while NS@HSA complexes can be triggered to release their drug payload using femtosecond near-IR laser illumination. Both complexes exhibit the potential for highly controlled drug release at the site of disease and within a narrow time window, unlike conventional chemotherapy. Such strategies could be used to increase the efficacy of chemotherapeutic treatment while lowering overall systemic dosages, reducing deleterious side effects.

Results and Discussion

Nanocomplex Synthesis and Characterization. Schematic representations of nanocomplex fabrication and the light-triggered drug-release process using two host biomolecules bound to Au NSs are shown in Scheme 1. To form the NS@DNA@drug nanocomplexes, *ds*DNA is first attached to NS through Au–thiol bonds. The DNA sequence selected for DTX (DNA1: 5′-HS-C_6H_{12}-GGA ATA CAC GCG CGA AAT CAC G-3′) is a variation of Dickerson's dodecamer, d(CGCGAATTCGCG)$_2$, which has previously been shown to complex taxol and other analogs (36). The base substitutions were made to result in the dsDNA structure having a higher melting point than any hairpin structures, which allows for preferential formation of the DNA duplex upon DNA cooling in the hybridization process. An adenine–thymine-rich sequence was chosen for LAP (DNA2 = 5′-HS-C_6H_{12}-AAA AAA ATA TAT AAT TAA AAG TTG AAA-3′). LAP's structure contains a pyrimidinamine, analagous to adenine, and is thus expected to bind to thymine in a similar manner (37). The NS@DNA@drug nanocomplexes are incubated with cells, then illuminated with a near-IR laser. The laser wavelength was selected to match the NS plasmon resonance in the near-IR spectral water window (38). To maximize drug-release efficiency, two illumination sources were investigated: CW laser irradiation and femtosecond pulsed-laser irradiation. CW illumination results in dehybridization of the DNA and release of the drug, while pulsed irradiation results in Au–S bond breakage and release of the dsDNA–drug complex.

HSA is the most abundant protein in blood plasma and can bind highly insoluble drug molecules in its hydrophobic pockets (39–41). Due to its large size and multiple binding regions, HSA has the potential to significantly increase the payload capacity of the nanocomplexes. NS are coated with HSA, which forms a protein corona around the particles, which are subsequently incubated with drug molecules (Scheme 1*B*). The NS@HSA@drug nanocomplexes are subsequently incubated with cells and irradiated with either a CW or pulsed near-IR laser in the same manner as the NS@DNA@drug nanocomplexes.

Functionalization of the NS surfaces was verified with transmission electron microscopy (TEM), extinction spectroscopy, zeta potential, and dynamic light scattering (DLS) (Fig. 1). The TEM images of unconjugated NS (orange) showed spherical particles with smooth regular surfaces, while TEM images of NS@DNA1 and NS@DNA2 (blue) showed the formation of a thin *ds*DNA layer around the NS (Fig. 1*A*). TEM images of NS@DNA1@DTX and NS@DNA2@LAP (green) showed no morphological changes (zoomed-in TEM images of the NS surface are seen in *SI Appendix*, Fig. S1). In the case of NS@HSA

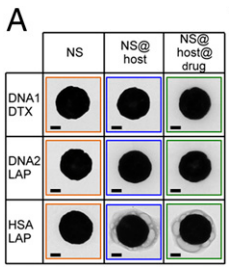

B

Sample	Extinction Maximum (nm)	Zeta Potential (mV)	Hydrodynamic Diameter (nm)
NS	766	-35.6 ± 0.3	178.7 ± 0.6
NS@DNA1	770	-46.2 ± 1.2	165.9 ± 1.2
NS@DNA1@DTX	774	-62.5 ± 0.8	155.4 ± 2.2
NS	771	-36.4 ± 0.9	176.1 ± 1.8
NS@DNA2	774	-42.2 ± 1.2	168.7 ± 1.4
NS@DNA2@LAP	779	-55.0 ± 1.1	163.7 ± 1.1
NS	771	-35.3 ± 0.5	177.5 ± 2.0
NS@HSA	788	-35.5 ± 0.9	180.8 ± 2.2
NS@HSA@LAP	786	-31.4 ± 0.6	178.9 ± 4.0

Fig. 1. Nanocomplex characterization. (*A*) TEM images of bare NS (orange), NS@host (blue), and NS@host@drug (green) for DNA1 scaffold–DTX drug, DNA2 host–LAP drug, and HSA host–LAP drug coatings. (Scale bars, 50 nm.) (*B*) Table of corresponding extinction maxima, zeta potentials, and hydrodynamic diameters with SD for scaffold and drug coatings.

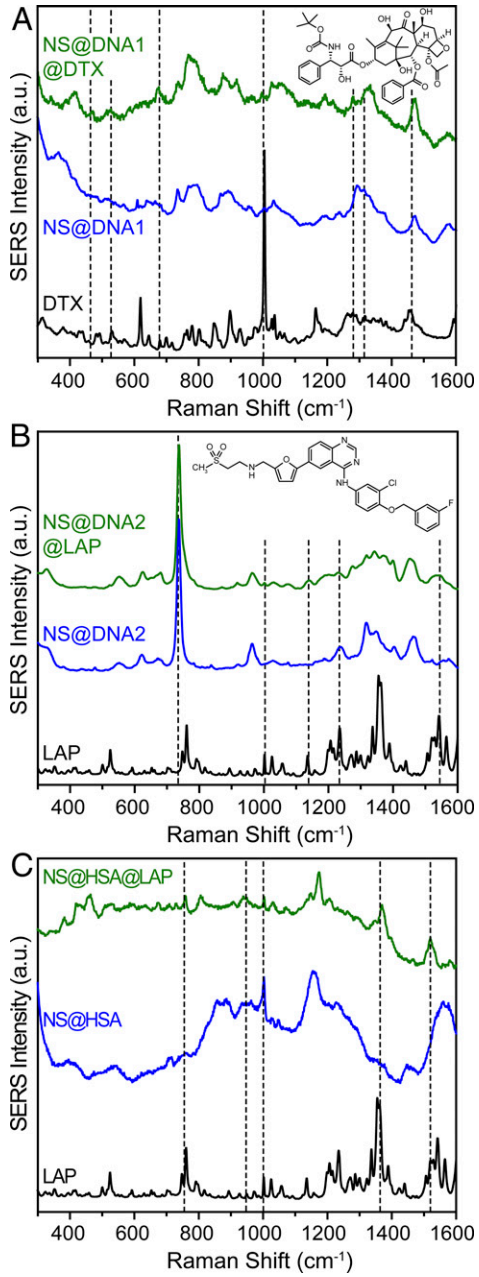

Fig. 2. SERS characterization to confirm drug loading. Normal Raman spectra of DTX (black) and LAP (black), and SERS spectra of NS@host (blue) and NS@host@drug (green) for (*A*) DNA1-DTX, (*B*) DNA2-LAP, and (*C*) HSA-LAP.

and NS@HSA@LAP (Fig. 1*A*), a hard and a soft corona around the NS can be observed in the TEM images of the complexes. The extinction maxima red-shift when coated with *ds*DNA and further red-shift when the drug molecules are loaded due to the changes in the dielectric environment around the NS (Fig. 1*B*). Protein coating induces a larger red-shift relative to *ds*DNA as a result of the larger size of the adsorbed protein layer. No changes in the peak shape or width of the extinction spectrum is observed, indicating that the nanocomplexes do not aggregate during the functionalization process. Zeta-potential measurements further confirm modification of the NS surface. For example, the zeta potential became more negative after *ds*DNA attachment and even more negative with drug loading (Fig. 1*B*). DLS measurements show the hydrodynamic diameter of bare NS decreases after DNA functionalization, possibly due to a change in the solvent from water to TE buffer. The hydrodynamic diameter further decreases after drug loading, likely as a result of compaction of the DNA (42). In the case of protein functionalization, the hydrodynamic diameter increases slightly after protein coating and shows minimal change upon drug loading.

Confirmation of Drug Loading. Surface-enhanced Raman spectroscopy (SERS) was used to confirm drug loading of the NS@host complexes (Fig. 2). The SERS spectrum of the thiolated *ds*DNA1 monolayer on the NS surface shows several characteristic SERS bands at 1,346 and 1,480 cm^{-1} (43). The SERS mode at 737 cm^{-1} is weak due to the low number of adenine bases in the DNA sequence (44) (Fig. 2*A*). Moreover, several strong SERS peaks at 1,003, 1,271, 1,520, and 1,543 cm^{-1} assigned to the benzene ring modes (νC-C, νC-O, νC = C, and ring stretching) are seen in the NS@DNA1@DTX SERS spectrum (45, 46). This indicates the DNA1–DTX complex formation. The bands at 1,340 and 1,475 cm^{-1} are enhanced in the complex spectrum in comparison with DNA1. In the case of the NS@DNA2 monolayer on the NS surface, the SERS spectrum is dominated by the adenine ring-breathing mode at 737 cm^{-1} (Fig. 2*B*). LAP Raman peaks including C-O-C mode of a substituted furan at 1,136 cm^{-1} are seen in the NS@DNA2@LAP SERS spectra. The protein–drug nanocomplex SERS data confirm that LAP has associated with the HSA protein corona on the particle surface from spectral features that include a quinazoline ring stretch at 1,369 cm^{-1} (Fig. 2*C*). The observed SERS frequencies and their assignments of DNA1, DNA2, and NS@DNA1@DTX, NS@DNA2@LAP complexes are listed in *SI Appendix*, Table S1.

Additional confirmation of LAP loading onto NS@DNA2 was performed with X-ray photoelectron spectroscopy (XPS) (*SI Appendix*, Fig. S2). A survey scan shows Au $4p^3$, $4d^3$, $4d^5$, $4f^5$, and $4f^7$ from the Au layer of the NS. Si 2s and 2p peaks, as well as O 1s peaks, originate from the SiO_2 core of the NS. The C 1s

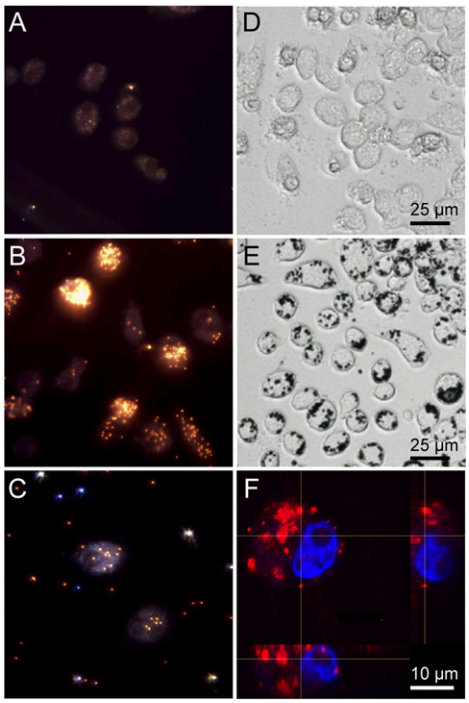

Fig. 3. Cellular uptake of nanocomplexes. Dark-field spectroscopy of NS@HSA incubated with RAW 264.7 cells for (*A*) 0 h, (*B*) 1 h, and (*C*) 4 h. Bright-field images (20× objective, four averages) measured in transmission (*D*) without and (*E*) with nanocomplexes. (*F*) Orthogonal view of the 3D maximum intensity projection image of cells incubated overnight with nanocomplex. Cells were stained for nucleus (Hoechst 33342, blue).

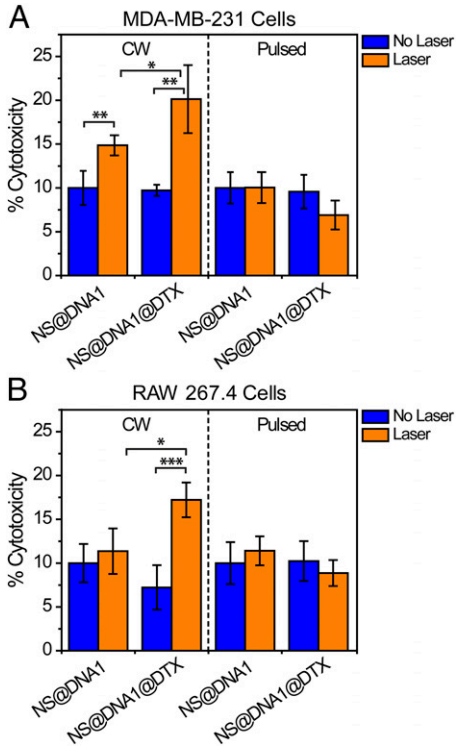

Fig. 4. Comparison of cell viability after DTX release from a DNA host without (blue) and with (orange) CW and pulsed lasers in (*A*) MDA-MB-231 and (*B*) RAW 264.7 cells. All samples were performed in replicates of four. Statistical significance is represented by the bars and asterisks where $*P < 0.05$, $**P < 0.01$, and $***P < 0.001$.

peak comes from the DNA. An elemental scan of the S 2p feature reveals a peak at a binding energy of 168 eV, indicating the presence of S in a sulfone group as opposed to a thiol, which further confirms LAP loading onto the DNA host.

Nanocomplex Cellular Uptake. Cellular uptake of the NS@host@drug complexes was investigated using dark-field, confocal, and reflectance (emission and extinction at 640 nm) microscopy in RAW 264.7 macrophage cells, and in MDA-MB-231-eGFP and SKBR3 breast cancer cells. For simplicity, only the RAW 264.7 images are shown (Fig. 3). In the dark-field images, internalization of the nanocomplexes can easily be seen as time-dependent, diffraction-limited bright spots (Fig. 3 *B* and *C*). As a control, cells not incubated with nanoparticles showed no observable bright spots (Fig. 3*A*). Because the dark-field images alone do not give clear evidence whether the NS@HSA@drug are adsorbed onto the outer membrane of the cells or internalized, bright-field images were also obtained. Varying the depth of field within an individual cell allows for clear 3D visualization of the nanocomplex distribution within the cell. Fig. 3*E* is a slice from the middle of the cell showing clear diffraction-limited dark spots corresponding to the nanocomplexes, verifying that the NS complexes are internalized within the cell. As a control, cells not incubated with the nanocomplexes showed no observable dark spots when imaged in the same mode (Fig. 3*D*). To further investigate the nanocomplex cellular uptake and localization inside the cells, confocal images were measured in transmission and reflection mode (emission and extinction at 640 nm) at varying depths. The details in the orthogonal YZ and XZ planes illustrate the location of the nanoparticles within the cell boundary around but not inside the nucleus [the nucleus was stained with Hoechst 33342 dye (Fig. 3*F*)]. We have previously shown that NS phagocytosed by macrophages are dispersed within vacuoles (34). TEM of a macrophage in the necrotic area of a breast tumor shows NS within a vacuole that is likely an endosome/lysosome (*SI Appendix*, Fig. S3).

Intracellular Light-Triggered Drug-Release Studies. Cellular cytotoxicity resulting from light-triggered release of DTX and LAP was evaluated using both the *ds*DNA and protein host adsorbates. Cells were grown for 24 h in 96-well plates, incubated for 4 h with nanocomplexes, washed with PBS, then given fresh media. Cells were irradiated with 1.5 W of CW laser power or a Ti:Sa laser amplifier (Coherent, RegA) operating at 250 kHz with an average power of 25 mW and 160-fs pulsed-laser power for 2 min, then incubated at 37 °C, 5% CO_2 for 24 h to allow time for the released drug molecules to interact with the cells. Cell death was evaluated with a lactate dehydrogenase (LDH) cytotoxicity assay. Percent cytotoxicity values were calculated considering 10% cell death in the control experiment, NS@host with no laser treatment.

DTX release from the DNA1 host was investigated in MDA-MB-231 breast cancer cells (Fig. 4*A*) and in RAW 264.7 macrophage cells (Fig. 4*B*). The NS@DNA1@DTX nanocomplex is shown to be nontoxic, since statistically no increase in cytotoxicity was observed compared with the NS@DNA1 nanoparticles. This indicates that DTX stays confined within the DNA host and that no leaching occurs. A very statistically significant ($P < 0.01$) increase in cytotoxicity for the cells with NS@DNA1 after CW

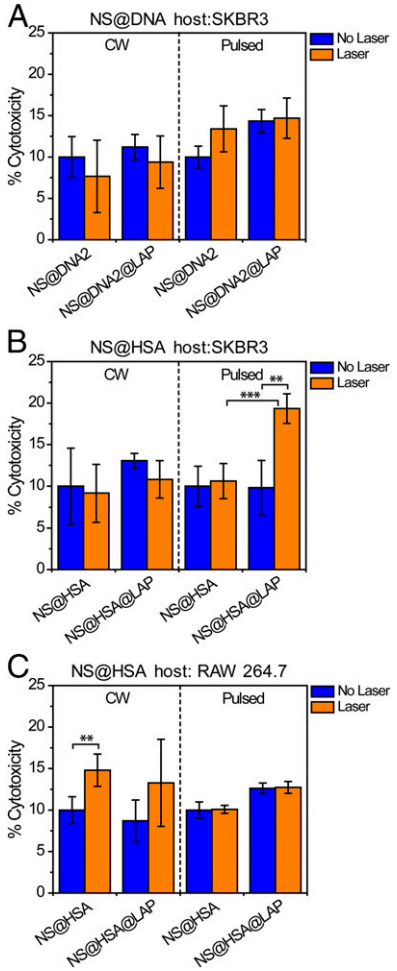

Fig. 5. Comparison of cell viability after LAP release in SKBR3 cells without (blue) and with (orange) CW and pulsed lasers from (*A*) a DNA host and (*B*) an HSA host. (*C*) Cell viability after LAP release in RAW 264.7 macrophage cells under CW and pulsed illumination. All samples were performed in replicates of four. Statistical significance is represented by the bars and asterisks where $**P < 0.01$ and $***P < 0.001$.

laser treatment (no DTX) is likely due to photothermal ablation. A statistically significant ($P < 0.05$) increase in cell death is observed under CW laser irradiation between no DTX and DTX, confirming there is a positive effect of drug release beyond any photothermal heating caused by the laser. A very statistically significant ($P < 0.01$) increase in cell death is seen when DTX is released with the CW laser compared with NS@DNA1@DTX with no laser, while no increased cell death is seen for pulsed-laser-induced release. This is most likely due to the different DNA release mechanisms resulting from CW vs. pulsed lasers (30). In the case of a CW laser, the nanocomplex and its surrounding local environment undergo a photothermal temperature increase, causing the *ds*DNA to dehybridize, releasing the drug and ssDNA. Similar results are seen for both the cancer and macrophage cells, which are to be expected, since DTX is not a targeted cancer drug and does not discriminate between cancerous and healthy cells. There is an extremely statistically significant ($P < 0.001$) increase in cytotoxicity for NS@DNA1@DTX without and with CW laser. In contrast, irradiation with a pulsed laser induces breakage of the Au–S anchoring bond of the *ds*DNA. As a result, the entire *ds*DNA–drug complex is released, with the drug likely remaining sequestered within the DNA: this should restrict DTX from inducing cell death upon irradiation.

In principle, pulsed-laser-induced drug release is preferable over CW laser-induced drug release, since far lower average powers can be used, minimizing photothermal heating effects that would include nonspecific cell death. Since pulsed-laser-induced drug release from the NS@DNA host releases the entire dsDNA–drug complex, NS@HSA was investigated as an alternative drug host. LAP was released from both an NS@DNA and NS@HSA host in SKBR3 breast cancer cells and RAW 264.7 macrophage cells. LAP was chosen to see if cell death could be preferentially induced in cancer cells over healthy cells, since LAP specifically targets the HER2 receptor that is overexpressed on SKBR3 cells. For the NS@DNA host, no statistically significant increase in cytotoxicity is observed for either CW or pulsed-laser-induced release for SKBR3 cells (Fig. 5*A*). There is also no increase in cytotoxicity for CW laser-induced release from the protein scaffold; however, there is a very statistically significant ($P < 0.01$) increase in cytotoxicity for pulsed-laser-induced LAP release from the NS@HSA host in SKBR3 cells (Fig. 5*B*). The low average power (25 mW) does not increase the local temperature and therefore cells with NS@HSA alone do not show increased death after pulsed-laser treatment. However, pulsed-laser irradiation is clearly sufficient to alter the HSA, releasing LAP from the NS@HSA@LAP nanocomplex, shown by the extremely statistically significant ($P < 0.001$) increase in cytotoxicity vs. pulsed irradiation of NS@HSA without LAP. The extent to which the NS-bound HSA is unfolded or denatured by femtosecond laser irradiation is unclear, and may be the subject of future studies.

LAP release was performed in the noncancerous macrophage cells as a control (Fig. 5*C*). Since macrophages lack the HER2 receptor, LAP release is not expected to induce cytotoxicity. There is a very statistically significant ($P < 0.01$) increase in cell death for NS@HSA with laser vs. no laser. This is likely due to photothermal heating. No selective increase in cytotoxicity for CW or pulsed-laser LAP release from the NS@HSA host was observed. The lack of increased cytotoxicity after LAP release from the NS@HSA host with a pulsed laser confirms that the laser treatment did not directly induce the cell death seen with the LAP release from the NS@HSA host for SKBR3 cells. This suggests that the released LAP can selectively induce cell death in HER2 expressing breast cancer cells, without affecting noncancerous cells.

Conclusion

Both CW and pulsed near-IR light have been shown to induce in vitro release of drug molecules from NS@DNA and NS@HSA complexes. DTX and targeted LAP, two commonly used breast cancer drugs, were released in both cancerous and noncancerous cells. The results demonstrate that there is a higher percent cytotoxicity for CW vs. pulsed-laser-induced DTX release from a DNA host; however, some nonspecific cell death is induced by the CW laser itself. Using the protein scaffold, increased cytotoxicity was observed for LAP release using pulsed vs. CW light in cancerous cells, while noncancerous cells were unaffected. These results show that light-triggered drug release could be a very promising method for delivering chemotherapy drugs in cancer treatment. By simply exchanging the chemotherapy drug, this system can be extended to treatments for many cancer types. The flexible loading and release strategies shown here will allow release to be more easily controlled and tailored for various chemotherapeutic drugs and cancer types. This in turn has the potential for increasing therapeutic efficacy by delivering high local drug concentrations while keeping systemic drug concentrations low, which would reduce the well-known deleterious side effects of conventional chemotherapeutic drug delivery methods. The hosting of LAP within HSA deserves specific comment. Tyrosine kinase inhibitors are notoriously insoluble in water, which is one of the reasons why this class of drug has poor oral bioavailability (47). Additionally, although clinical trials have demonstrated that the combination of LAP with other HER2 directed therapies for dual blockade is of benefit in certain subgroups of patients (48), severe toxicities, diarrhea in particular, are leading to poor compliance and treatment discontinuation (49). The NS@HSA@LAP formulation has the potential to deliver an efficacious dose of a poorly soluble drug directly to the tumor where it can be released. As it will be released only at the tumor, theoretically the systemic dose will be less than with current oral formulations resulting in less toxicity, more compliance, and greater disease control.

Materials and Methods

The following information is available in *SI Appendix*: TEM images and extinction spectra illustrating DNA and LAP coatings around NS (*SI Appendix*, Fig. S1); SERS peak assignments for the attachment of DNA, HSA, DTX, and LAP to NS surfaces (*SI Appendix*, Table S1); XPS characterization of NS@DNA and NS@DNA@LAP (*SI Appendix*, Fig. S2); TEM of infiltration of monocytes/macrophages loaded with NS in breast tumor tissue (*SI Appendix*, Fig. S3); CD characterization of DNA1, DNA1-DTX, DNA2, and DNA2-LAP (*SI Appendix*, Fig. S4); and percent cytotoxicity of cells incubated with varying drug concentrations (*SI Appendix*, Table S2).

ACKNOWLEDGMENTS. We thank Dr. Sandra W. Bishnoi, Nate Hogan, and Linan Zhou for helpful discussions and editing. This work was financially supported by the Robert A. Welch Foundation (C-1220), J. Evans Attwell-Welch Fellowship (L-C-0004), Congressionally Directed Medical Research Program Grant W81 XWH-13-1-0341, Air Force Office of Scientific Research: Multidisciplinary Research Program of the University Research Initiative Grant FA 9550-15-1-0022, and the National Science Foundation (NSF) Graduate Research Fellowship under Grant 0940902. Any opinion, findings, and conclusions or recommendations expressed in this material are those of the authors and do not necessarily reflect the views of the NSF.

1. Torre LA, et al. (2015) Global cancer statistics, 2012. *CA Cancer J Clin* 65:87–108.
2. von Eschenbach AC (2004) A vision for the National Cancer Program in the United States. *Nat Rev Cancer* 4:820–828.
3. Chabner BA, Roberts TG, Jr (2005) Timeline: Chemotherapy and the war on cancer. *Nat Rev Cancer* 5:65–72.
4. Anker JN, et al. (2008) Biosensing with plasmonic nanosensors. *Nat Mater* 7:442–453.
5. Huang X, El-Sayed MA (2010) Gold nanoparticles: Optical properties and implementations in cancer diagnosis and photothermal therapy. *J Adv Res* 1:13–28.
6. Ayala-Orozco C, et al. (2014) Au nanomatryoshkas as efficient near-infrared photothermal transducers for cancer treatment: Benchmarking against nanoshells. *ACS Nano* 8:6372–6381.
7. Loo C, et al. (2004) Nanoshell-enabled photonics-based imaging and therapy of cancer. *Technol Cancer Res Treat* 3:33–40.
8. Thanh NTK, Green LAW (2010) Functionalisation of nanoparticles for biomedical applications. *Nano Today* 5:213–230.
9. Wilhelm S, et al. (2016) Analysis of nanoparticle delivery to tumours. *Nat Rev Mater* 1:16014.

10. Xiao Z, et al. (2012) DNA self-assembly of targeted near-infrared-responsive gold nanoparticles for cancer thermo-chemotherapy. *Angew Chem Int Ed Engl* 51: 11853–11857.
11. Loo C, Lowery A, Halas N, West J, Drezek R (2005) Immunotargeted nanoshells for integrated cancer imaging and therapy. *Nano Lett* 5:709–711.
12. O'Neal DP, Hirsch LR, Halas NJ, Payne JD, West JL (2004) Photo-thermal tumor ablation in mice using near infrared-absorbing nanoparticles. *Cancer Lett* 209:171–176.
13. Gad SC, Sharp KL, Montgomery C, Payne JD, Goodrich GP (2012) Evaluation of the toxicity of intravenous delivery of auroshell particles (gold-silica nanoshells). *Int J Toxicol* 31:584–594.
14. Huschka R, et al. (2012) Gene silencing by gold nanoshell-mediated delivery and laser-triggered release of antisense oligonucleotide and siRNA. *ACS Nano* 6:7681–7691.
15. Barhoumi A, Huschka R, Bardhan R, Knight MW, Halas NJ (2009) Light-induced release of DNA from plasmon-resonant nanoparticles: Towards light-controlled gene therapy. *Chem Phys Lett* 482:171–179.
16. Huschka R, Neumann O, Barhoumi A, Halas NJ (2010) Visualizing light-triggered release of molecules inside living cells. *Nano Lett* 10:4117–4122.
17. Singhana B, Slattery P, Chen A, Wallace M, Melancon MP (2014) Light-activatable gold nanoshells for drug delivery applications. *AAPS PharmSciTech* 15:741–752.
18. Pérez-Herrero E, Fernández-Medarde A (2015) Advanced targeted therapies in cancer: Drug nanocarriers, the future of chemotherapy. *Eur J Pharm Biopharm* 93:52–79.
19. Ahumada M, et al. (2017) Association models for binding of molecules to nanostructures. *Analyst* 142:2067–2089.
20. Wicki A, Witzigmann D, Balasubramanian V, Huwyler J (2015) Nanomedicine in cancer therapy: Challenges, opportunities, and clinical applications. *J Control Release* 200:138–157.
21. Shi J, Kantoff PW, Wooster R, Farokhzad OC (2017) Cancer nanomedicine: Progress, challenges and opportunities. *Nat Rev Cancer* 17:20–37.
22. Mirkin CA, Letsinger RL, Mucic RC, Storhoff JJ (1996) A DNA-based method for rationally assembling nanoparticles into macroscopic materials. *Nature* 382:607–609.
23. Dietz GPH, Bähr M (2004) Delivery of bioactive molecules into the cell: The Trojan horse approach. *Mol Cell Neurosci* 27:85–131.
24. Maham A, Tang Z, Wu H, Wang J, Lin Y (2009) Protein-based nanomedicine platforms for drug delivery. *Small* 5:1706–1721.
25. Davis ME, Chen ZG, Shin DM (2008) Nanoparticle therapeutics: An emerging treatment modality for cancer. *Nat Rev Drug Discov* 7:771–782.
26. Chan WCW (2007) *Bio-Applications of Nanoparticles* (Landes Bioscience and Springer Science+Business Media LLC, New York), pp 48–56.
27. Rana S, Bajaj A, Mout R, Rotello VM (2012) Monolayer coated gold nanoparticles for delivery applications. *Adv Drug Deliv Rev* 64:200–216.
28. Gao H, et al. (2013) Ligand modified nanoparticles increases cell uptake, alters endocytosis and elevates glioma distribution and internalization. *Sci Rep* 3:2534.
29. Zolnik BS, González-Fernández A, Sadrieh N, Dobrovolskaia MA (2010) Nanoparticles and the immune system. *Endocrinology* 151:458–465.
30. Goodman AM, et al. (2017) Understanding resonant light-triggered DNA release from plasmonic nanoparticles. *ACS Nano* 11:171–179.
31. Dumontet C, Jordan MA (2010) Microtubule-binding agents: A dynamic field of cancer therapeutics. *Nat Rev Drug Discov* 9:790–803.
32. Taskar KS, et al. (2012) Lapatinib distribution in HER2 overexpressing experimental brain metastases of breast cancer. *Pharm Res* 29:770–781.
33. American Cancer Society (2016) Targeted therapy for breast cancer. Available at https://www.cancer.org/cancer/breast-cancer/treatment/targeted-therapy-for-breast-cancer.html. Accessed April 17, 2016.
34. Choi M-R, et al. (2007) A cellular Trojan horse for delivery of therapeutic nanoparticles into tumors. *Nano Lett* 7:3759–3765.
35. Choi MR, et al. (2012) Delivery of nanoparticles to brain metastases of breast cancer using a cellular Trojan horse. *Cancer Nanotechnol* 3:47–54.
36. Krishna AG, Kumar DV, Khan BM, Rawal SK, Ganesh KN (1998) Taxol-DNA interactions: Fluorescence and CD studies of DNA groove binding properties of taxol. *Biochim Biophys Acta* 1381:104–112.
37. Dogan-Topal B, Bozal-Palabiyik B, Ozkan SA, Uslu B (2014) Investigation of anticancer drug lapatinib and its interaction with dsDNA by electrochemical and spectroscopic techniques. *Sens Actuators B Chem* 194:185–194.
38. Weissleder R (2001) A clearer vision for in vivo imaging. *Nat Biotechnol* 19:316–317.
39. Larsen MT, Kuhlmann M, Hvam ML, Howard KA (2016) Albumin-based drug delivery: Harnessing nature to cure disease. *Mol Cell Ther* 4:3.
40. Agudelo D, et al. (2012) Probing the binding sites of antibiotic drugs doxorubicin and N-(trifluoroacetyl) doxorubicin with human and bovine serum albumins. *PLoS One* 7: e43814.
41. Petitpas I, Bhattacharya AA, Twine S, East M, Curry S (2001) Crystal structure analysis of warfarin binding to human serum albumin: Anatomy of drug site I. *J Biol Chem* 276:22804–22809.
42. Cheng C, Ran S-Y (2014) Interaction between DNA and trimethyl-ammonium bromides with different alkyl chain lengths. *Sci World J* 2014:863049.
43. Kast RE, et al. (2008) Raman spectroscopy can differentiate malignant tumors from normal breast tissue and detect early neoplastic changes in a mouse model. *Biopolymers* 89:235–241.
44. Barhoumi A, Halas NJ (2010) Label-free detection of DNA hybridization using surface enhanced Raman spectroscopy. *J Am Chem Soc* 132:12792–12793.
45. Cipriani P, Ben-Amotz D (2005) Characterization of select members of the taxane family using Raman spectroscopy. *J Raman Spectrosc* 36:1052–1058.
46. Devi TSR, Gayathri S (2010) FTIR And FT-Raman spectral analysis of paclitaxel drugs. *Int J Pharm Sci Rev Res* 2:106–110.
47. Herbrink M, Nuijen B, Schellens JH, Beijnen JH (2015) Variability in bioavailability of small molecular tyrosine kinase inhibitors. *Cancer Treat Rev* 41:412–422.
48. Clavarezza M, et al. (2016) Dual block with lapatinib and trastuzumab versus single-agent trastuzumab combined with chemotherapy as neoadjuvant treatment of HER2-positive breast cancer: A meta-analysis of randomized trials. *Clin Cancer Res* 22: 4594–4603.
49. Hao S, et al. (2017) Does dual HER-2 blockade treatment increase the risk of severe toxicities of special interests in breast cancer patients: A meta-analysis of randomized controlled trials. *Oncotarget* 8:19923–19933.